Copyright
by
Vincent Roathy Heng
2015

The Thesis Committee for Vincent Roathy Heng
certifies that this is the approved version of the following thesis:

Energy Focused Modeling and Optimization of a Radiant Tube Roller Hearth Austenization Furnace

APPROVED BY

SUPERVISING COMMITTEE:

Michael Baldea, Supervisor

Thomas F. Edgar, Co-Supervisor

Energy Focused Modeling and Optimization of a Radiant Tube Roller Hearth Austenization Furnace

by

Vincent Roathy Heng, B.S.

THESIS

Presented to the Faculty of the Graduate School of

The University of Texas at Austin

in Partial Fulfillment

of the Requirements

for the Degree of

MASTER OF SCIENCE IN ENGINEERING

THE UNIVERSITY OF TEXAS AT AUSTIN

May 2015

Dedicated to my grandmother

Acknowledgments

First, I thank my advisor, Dr. Michael Baldea, for believing in my ability and providing a source of wisdom in my research endeavors. My research productivity and achievements are a direct result of the mentoring I received from him. I also thank Dr. Thomas F. Edgar and Dr. Ofodike A. Ezekoye, both of whom I frequently discussed research questions and problems with.

I acknowledge collaborating efforts from Andrew Kurzawski for assisting in radiation based modeling, especially the view factor function, and Ankur Kumar for his timeless support. Additionally, my labmates as a whole in the Baldea and Edgar groups have been a great family to me in my time at the University of Texas. Especially helpful were Matt Walters, Bo Lu, and Corey James, and I am grateful for their advice and comradery.

I acknowledge those at UCLA who gave me a passion for research, specifically, Dr. Gerassimos Orkoulas as my undergraduate advisor and Dr. Michael Nayhouse as my graduate student mentor. Additionally, I thank Bob Lamm, Harding Luan, and Andrew Segal as people I modeled my research vigor around. I thank my friends Shuyang Fang, Darren Dalton, Paresh Dave, Marc Bauthier, Kyle Ueyama, and Jason Ang for their eternal friendship.

Lastly, I thank the guidance of my family. I thank my father, Kim, for instilling a love of science and engineering to me, my mother, Sochitra, for the nurture and care in growing up, and my sister, Kanya, for being the test child and defining a path to success. I finally thank my best friend Lauren Davis for all of the love and support.

First in this thesis, the energy usage problem in the United States is framed. Specific to this thesis, the metal processing industry uses 2 quadrillion BTU per year primarily from furnaces such as the heat treating furnace considered here, and over half this energy is lost as waste heat. Next, the modeling methodology used for this thesis is detailed. Radiosity based techniques are used to model the high temperature surface-to-surface interactions present in the furnace. Case studies are done for the furnace under constant fuel input and additionally under temperature set point control. The model is then used to find the optimal temperature set points to operate the furnace efficiently from an energy standpoint while maintaining steel part properties. The future of this research project is considered. Model validation will be performed, and there is potential for model predictive control to be implemented on the system. The thesis is concluded with an overview of results and a note on the application of the methodologies to the plant.

The first three chapters constitutes work presented at the 2014 AIChE Annual Meeting in Atlanta, GA. Elements of the fourth chapter were presented at the 2015 Texas-Wisconsin-California Control Consortium in Austin, Texas. A paper covering the work of this thesis will be submitted for publication shortly after the submission of this thesis. This manuscript will be authored by Vincent R. Heng, Andrew Kurzawksi, Thomas F. Edgar, Ofodike A. Ezekoye, and Michael Baldea. Andrew Kurzawski implemented the view factor function, and Thomas F. Edgar, Ofodike A. Ezekoye, and Michael Baldea advised the research.

Energy Focused Modeling and Optimization of a Radiant Tube Roller Hearth Austenization Furnace

Vincent Roathy Heng, M.S.E.
The University of Texas at Austin, 2015

Supervisors: Michael Baldea
Thomas F. Edgar

In this thesis, we develop a two-dimensional energy-focused model of a roller hearth heat treating furnace. The two-dimensional model is based on first-principles, detailed representations of radiation with non-participating gas and convective heat transfer. The model computes the exit temperature profile of the treated steel parts while calculating the energy consumption and efficiency of the furnace. We propose a dual iterative numerical scheme to solve the model, and validate its efficacy by simulating the dynamics of the furnace during startup and cool-down, as well as for steady-state operation. We first present two case studies to show the capability of the model in simulating the furnace system with constant fuel input to the burners. We then implement feedback control on the model to maintain furnace temperatures by manipulating the fuel feed rate to the furnace burners. A case study using suggested temperature set points from the plant details energy consumption within the furnace under control. We then use the model to find the optimal set points to minimize energy consumption while ensuring certain part temperature properties are met when part processing is complete. With optimized set points, 8.5% less energy per part is required versus the heuristic set points.

Table of Contents

List of Tables

List of Figures

Chapter 1

Introduction

Overall energy consumption in the United States totals around 100 quadrillion BTU (quads) per year since the 2000s, peaking at 101 quads in 2007 [United States Energy Information Administration, 2014]. The industrial sector accounts for approximately one-third of energy usage, or 30 quads [Stones et al., 2007]. Under the industrial sector umbrella, metal processing is the fourth largest primary energy user with yearly demands of 2 quads [Viswanathan et al., 2005]. The energy demands are primarily related to fuel for furnaces and boilers [Pellegrino et al., 2004].

For an individual metal processing plant, reheating and heat treating furnaces account for 65% to 80% of the overall energy use [Thekdi, 2010]. Heat treating induces toughness, shear strength, and tensile strength to parts and compound steel. Energy demands for this process are 1.6 mmBTU to 1.8 mmBTU per ton of processed steel [Thekdi, 2010]. The energy demands are intensified due to net furnace efficiency ranging from 20% to 60% and gross fuel input to load efficiency of 20% to 40% [Thekdi, 2010]. Moreover, in practice, operators tend to heuristically overcompensate heating requirements to ensure a minimum part temperature threshold is reached (we note that, in general, readings of part temperatures, especially in the interior of the parts, are not available, whether inside the furnace or at the furnace exit).

The large intrinsic energy demand, combined with typically low process

efficiency make heat treating furnaces a primary target for advanced, model-based control. A model is needed to understand the physical phenomena occurring within the furnace, and for estimating product temperatures as a function of time, position in the furnace, and burner fuel input. Developing an accurate, energy management-focused model is difficult due to radiation-induced nonlinearities, large time constants, and complex furnace geometries which, in turn, lead to short and long-distance interactions between the furnace structure and the processed parts.

In the present thesis, we focus on developing such a mathematical model for a roller hearth furnace. The furnace (Figure 1.1), is a continuous process; steel parts are loaded onto trays and conveyed through a heated tunnel. The residence time within the furnace is in the order of hours. Since heat treating is a finishing step in the overall metal processing workflow, the furnace is indirectly fired, with fuel combustion occurring in radiant tube burners. Nitrogen is injected into the furnace to create an inert atmosphere and prevent surface oxidation of the steel. The furnace operates at temperatures in excess of $1600^{\circ}F$ (approximately $1150K$).

This model is designed to evaluate energy usage within the furnace, as well as part temperatures. The model inputs are the physical properties and dimensions of the steel parts, fuel flow rates to the radiant tube burners, set point temperatures of the furnace zones, and the condition of the surrondings of the furnace. In view of control applications and deployment in practice, we aim to develop a model structure that can be easily adapted to other systems by adjusting a a reasonable number of parameters.

The goal of this thesis is to properly model the roller hearth system, then to search for optimal operating conditions. First, we discuss the radiation

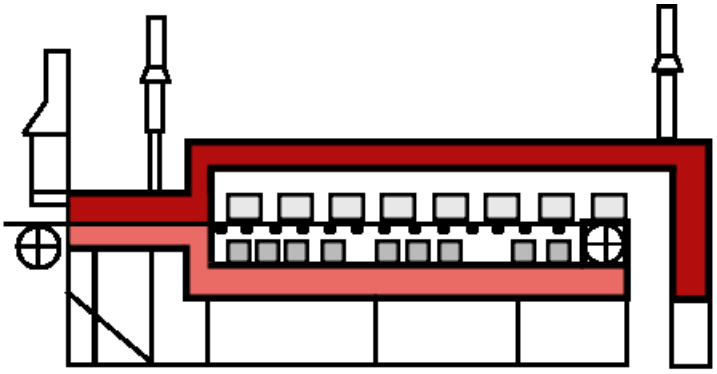

Figure 1.1: Prototype furnace schematic for roller hearth furnace. Metal parts are heated by combustion of natural gas in radiant tube burners. After this furnace, the parts are placed into an oil quench bath to induce the crystal structure change and give the parts properties such as hardness, shear strength, and tensile strength. Based on schematic by AFC-Holcroft [Holcroft].

model (Section 2.3) used to describe the system. With the mathematical model fully described, we then show case studies for furnace operation with constant fuel input (Section 3.2). Our next step is to implement temperature control on the furnace in the same manner as the plant (Section 4.1) and perform simulations using plant temperature set points. Our final work is searching for the optimal set points using response surface surrogate models to achieve desired part properties upon exit, while minimizing the overall energy use of the furnace (Section 4.2). In doing this, we are able to achieve an 8.5% energy savings over the heuristic method (operation based on operator experience, rather than a detailed, mathematical foundation). This is in large part due to the increased knowledge the model gives to the process, where the steel temperatures are now known rather than inferred in the real process. This contribution is unique in the detailed energy approach of the system, rather than temperature tracking or broad energy monitoring, which we discuss in

the following Literature Review.

1.1 Literature Review

Previous literature studies on metal processing furnaces of this type are centered on pusher-type slab reheating systems (for example, see Ramamurthy et al. [1995]). While geometrically similar to the roller hearth heat treating furnace considered here, reheating furnaces are commonly direct-fired, and their mathematical models must consider gas-to-surface radiation interactions. As we will discuss later, these interactions can be neglected for the present class of systems, where only surface-to-surface interactions will be considered, resulting in a different radiation model. Moreover, due to the fact that reheating is a pre-finishing step, contact between the (unfinished) parts is allowed in reheating furnaces. This allows modeling pusher-type furnaces as two independent domains, a lower furnace and an upper furnace, and consider only wall-to-slab and burner-to-slab interactions (ignoring wall-to-wall interactions). In many cases, the slab is considered thin enough to be approximated as a one-dimensional system.

By contrast, the heat treating roller hearth furnace considered in this thesis is designed to process forged steel parts, rather than raw steel slabs. The parts are placed in the furnace at some distance from each other and, as a consequence, interactions between like surfaces must be taken into account; this includes part-to-part interactions as well as interactions between the ceiling and floor of the furnace. Whereas gas-to-surface radiation models capture short distance radiation interactions with reasonable accuracy, when considering surface-to-surface radiation, long distance effects must be considered to completely characterize energy use.

The modeling of furnaces is further complicated by nonlinearities that arise from modeling radiative heat transfer with relatively complex furnace and part geometries. As a consequence, furnace modeling efforts have followed three main approaches, which we review below:

- **Black-Box** (typically neural network) models are a common empirical technique for modeling reheating furnaces. Liao et al. [2006] used a radial basis function neural network due to its simple structure. The model was successful in predicting furnace temperature with varying operating conditions, but slab temperature was not considered. This model also did not consider the energy usage of the furnace, and is likely better suited for process monitoring. Xuegang et al. [2009] followed a similar path, and proposed using pattern swarm and particle swarm optimization to train the neural network model. Kim et al. [1998] proposed using a mixture of expert networks with principal component analysis to reduce model dimensionality. Laurinen and Röning [2005] used neural networks to predict surface slab temperatures at the furnace exit. Since neural-network models are entirely data-driven, it is typically not possible use them to predict internal part temperatures. This is a significant shortcoming when it comes to modeling heat treating furnaces, since the internal temperature distributions are a deciding factor in the part quality obtained following oil quenching [Pan et al., 2002].

- **Computational fluid dynamics** (CFD) simulations are the approach of choice for high-fidelity modeling of furnace systems. Tang et al. [2010] used CFD to analyze gas flow patterns and temperatures within a pusher-slab furnace. Further results were obtained by Triebl et al. [2014],

who analyzed both the gas and the furnace wall temperatures within a pusher-slab furnace. Details such as the phase transition of steel to its different allotropes can be considered along with the thermal stresses associated with the reheating process as shown in the work by Pan et al. [2002]. However, CFD simulations are computationally intensive, and detailed results are obtained at the cost of long simulation runs (which can extend for several days even when using high-performance computing equipment). This, in turn, limits the use of such models for online applications such as real-time control and optimal energy management. Moreover, we note that details such as gas flow patterns and velocity distributions are typically not needed and/or directly useful in such applications.

- **Equation-oriented modeling** bridges empirical and CFD approaches. Modeling equations are based on first-principles, but several assumptions and approximations are made to simplify the system while preserving the characteristics that are important for the purpose of the model. In this area, we recall the work of Balbis et al. [2008], focusing on predicting part temperatures at the furnace exit. In this work, the furnace was discretized into a series of well-mixed control volumes, disregarding long-range interactions. Yang and Lu [1986] approached furnace model development in a similar manner, by combining the temperature measurements from the top and bottom regions of the furnace into a single variable; moreover, a linearized version of the radiation heat transfer relations was proposed. In the work by Steinboeck et al. [2010], the load temperature profile was assumed to be one-dimensional, and finite element approximations were used to solve for only key part temperature

information, without solving for the part temperature profile explicitly. Likewise, Yoshitani et al. [1994] and Mochida et al. [1997] simplified the radiation relationships from furnace surface-to-load to only consider the direct, short range interactions. Kang et al. [2007] also simplified modeling efforts by using empirical coefficients found from experimental results to be lumped into the emissivity term in the radiation equation.

Models of this type are typically developed with control applications in mind, focusing on determining the fuel input required to maintain a desired furnace (and/or part) temperature (see also, e.g., Pike Jr and Citron [1970]). Yang and Lu [1988] used a previously developed model [Yang and Lu, 1986] to perform a dynamic optimization of furnace operation. Additionally, Steinboeck et al. [2011] used their model [Steinboeck et al., 2010] to predict slab temperature as a function of furnace temperatures for model-based control purposes. It is important to notice, however, that simplifications such as omitting long-range radiation effects and lumping large portions of the physical domain in single variables can cause these models to produce inaccurate results when attempting to predict and optimize furnace energy use. These simplifications are not valid for the furnace considered in this thesis, where surface-to-surface radiation is the dominant form of heat transfer.

In the present work, we focus on developing an energy-oriented model for a heat treating furnace. We will work within the equation-oriented paradigm described above.

Our contribution represents a departure from the publications reviewed above, because, i) we consider an indirectly fired heat treating furnace, and, ii)

we account for long-range radiation interactions. Moreover, consider indirect heating with radiant tube burners, which precludes using an approximation based on lumped, isothermal control volumes as proposed, e.g, by Chen et al. [2005] and Han et al. [2011]. These features increase model size, and our efforts also focus on the numerical solution aspects, in view of future incorporation of the proposed model in online control and energy optimization applications.

Chapter 2

Model Development

2.1 Plant Testbed

The physical system that this work is based on is a steel processing plant operated by General Dynamics in Scranton, Pennsylvania. We will refer to this as the "plant." In this plant, raw steel slabs are first heated in an open-fired rotary furnace. The steel is then sent to a forging line where the raw steel slabs are formed into the desired shape. The forged steel parts are then placed onto trays and sent to the austenitization line, which is the furnace we consider here. The austenitization furnace is used to heat the steel to a high temperature, without oxidizing the surface. The parts are then quenched in an oil bath, where the desired steel properties such as ductile strength and hardness are induced. After cooling, the steel parts are ready to be shipped out. At intermediate stages within the process, select steel parts from the batches are tested to ensure proper processing. This is done due to a lack of sensing on each steel part in itself.

While high steel throughput capacity is valuable for future needs, the plant is oversized for current demands. As a result, any energy savings possible, especially during production downturn, are helpful. We will look at the roller hearth austenitization furnace in this work, which is a primary user of energy in the overall process.

2.2 Model Assumptions

We base our work on the system presented in Figure 1.1. The furnace is heated using ceiling and floor burners; adjacent burners (both ceiling and floor) are grouped together for temperature control purposes, in the sense that the fuel flow rate to these groups, which reside in the same *temperature control zone*, is changed simultaneously. We begin by deriving an abstraction of the furnace geometry based on a minimal set of reasonable assumptions, after which we describe the mathematical model equations and the associated numerical solution strategy.

(A1) We build our model around a two-dimensional geometry shown in Figure 2.1. A similar assumption was made by other authors (including, e.g., Ramamurthy et al. [1995], Steinboeck et al. [2010], and Panjkovic and Gloss [2012]) in order to balance computational efficiency with the ability to capture long range radiation interactions.

(A2) Parts subject to heat treating are loaded on a tray that is conveyed through the furnace. We will neglect the interactions between the parts loaded on an individual tray and refer to the ensemble of the tray and its contents as a "part." We will model this ensemble as a rectangular structure with equivalent metal mass.

(A3) Due to the spacing between rollers, we assume that conduction does not play a major role in the heat exchange between parts. Thus, we only model radiation and convection. We also assume that the mass of the conveyor belt is small compared to that of the part, and exclude the conveyor belt from our model.

(A4) In practice, a nitrogen blanket is created in the furnace to prevent surface oxidation of the parts. Since nitrogen is a diatomic molecule, there is no gas-to-surface radiation interaction [Incropera, 2011], and only surface-to-surface radiation heat exchange is considered.

(A5) The furnace is discretized into a series of control volumes for simulation purposes. Control volumes are used to calculate a discrete gas temperature profile within the furnace.

2.3 Radiosity Heat Transfer

Due to the high operating temperatures, radiation is the primary mode of heat transfer in the furnace. To facilitate modeling radiative heat transfer, we discretize the geometric elements of the furnace (including the burner panels, refractory insulation, and the load parts) into a set of surfaces. Considering the diagram shown in Figure 2.1, the furnace is discretized into subsurfaces based on burner panels and refractory insulation. When parts are within the furnace, each surface of each part is included as an additional surface the radiation model. For every surface $i \in N$, with N being the total number of surfaces (note that the number of surfaces changes as parts are loaded to or exit the furnace, an aspect that we discuss in detail later in the thesis), we write an energy balance equation as follows:

$$Q_{net,i} = Q_{radiation,i} + Q_{convection,i} \quad i \in N \tag{2.1}$$

where $Q_{net,i}$ is the overall heat to a surface (whose definition depends on the surface type). Then, the radiosity, J_i, defines the net amount of heat leaving

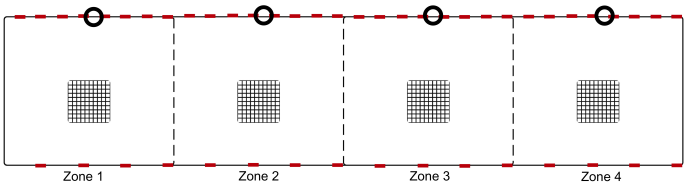

Figure 2.1: Furnace model structure. The black lines represent insulating walls, the red lines burner panels, and the hatched rectangle load. The dotted lines indicate the boundary between furnace zones, i.e. temperature control zones within the furnace in real operation. The circled subsurface is the surface we use for control (see Section 4.1). In this diagram, the parts are loaded on the left hand side and exit on the right hand side, and nitrogen is fed from the right hand side and exits at the left.

surface i via radiation. The heat from radiation is given by two relationships [Incropera, 2011]:

$$Q_{radiation,i} = \frac{\sigma T_i^4 - J_i}{\frac{1-\epsilon_i}{\epsilon_i A_i}} \tag{2.2}$$

and

$$Q_{radiation,i} = \sum_{j=1}^{N} \frac{J_i - J_j}{(A_i F_{i,j})^{-1}} \tag{2.3}$$

where σ is the Stefan-Boltzmann constant, ϵ_i is the emissivity of surface i, and $F_{i,j}$ is the value of the view factor from surface j to surface i, as will be described later in Section 2.3.1. Combining Equation 2.1 with Equations 2.2 and 2.3, the net heat for a surface i within the furnace becomes:

$$Q_{net,i} - h_{furn} A_i \left(T_i - T_w^{\infty}\right) = \frac{\sigma T_i^4 - J_i}{\frac{1-\epsilon_i}{\epsilon_i A_i}} \quad i \in N \tag{2.4}$$

$$Q_{net,i} - h_{furn} A_i \left(T_i - T_w^{\infty}\right) = \sum_{j=1}^{N} \frac{J_i - J_j}{(A_i F_{i,j})^{-1}} \quad i \in N \tag{2.5}$$

Equation 2.4 is used for burner surfaces and Equation 2.5 is used for insulating walls as well as part surfaces. This is due to the fact that burners generate heat and, as a consequence, $Q_{net,i}$ is a system input, while for the other surfaces $Q_{net,i}$ is an output. The additional term, $h_{furn}A_i\left(T_i - T_w^{\infty}\right)$, captures convective heat transfer with the nitrogen gas flowing in the furnace. The temperature of the gas phase in control volume w is T_w^{∞}. The heat transfer coefficient within the furnace, h_{furn}, is computed from the Nusselt and Prandtl numbers (Nu and Pr, respectively) as follows:

$$Re = \frac{\dot{m}_{N_2} D_h}{\mu} \tag{2.6}$$

$$Nu = 0.023 Re^{0.8} Pr^{0.4} \tag{2.7}$$

$$h_{furn} = \frac{k_{N_2} Nu}{D_h} \tag{2.8}$$

$$D_h = \frac{4A}{P} \tag{2.9}$$

In these equations, the Reynolds number, Re is found from the hydraulic diameter, D_h, and the mass flow rate. A is the cross sectional area of the furnace perpendicular to mass flow and P is the perimeter. The Prandtl number, Pr, is assumed to be a property of the gas [Incropera, 2011].

The first relationship, Equation 2.4, relates the overall heat balance with the difference between the temperature of surface i and its radiosity, J_i. The denominator in the right hand side of the equation is a thermal resistance as a function of emissivity and area. The second relationship, Equation 2.5, relates the overall heat balance with the difference in radiosities of the active surface i with every other surface in the furnace. There is a resistance term for this difference which involves the area as well as $F_{i,j}$, which is the view factor,

or sight line, of surface i to surface j (see the following section on view factor calculation).

Equations (2.4)-(2.5) constitute a system of $2N$ equations with $2N$ unknowns (i.e., the temperatures T_i and radiosities J_i, $i = 1, \ldots, N$ of each surface). In what follows, we provide further details on the problem definition, and we address the solution of this system.

2.3.1 View Factor Calculation

To calculate the view factor matrix $F_{i,j}$ between surfaces, each surface is discretized into k sub-surfaces and the view factor between each sub-surface and full surface is calculated using Hottel's crossed string method [Derrick, 1985].

$$F_{i,j} = \frac{AD + BC - AC - BD}{2A_i} \tag{2.10}$$

In this equation, AD and BC are the distances between end points of surfaces A_i and A_j where the lines cross, whereas AC and BD are the edge to edge distances. In the limit as the area of surface i approaches zero, this formula becomes

$$F_{i,j} = \frac{sin\psi_2 - sin\psi_1}{2A_i} \tag{2.11}$$

Applying this principle to each sub-surface (A_{ik}), we can calculate the view factors $F_{ik,j}$ for all k, where the total view factor is a sum of sub-surface view factors weighted by the corresponding areas

$$F_{i,j} = \sum_{k} \frac{F_{ik,j}}{A_{ik}} \tag{2.12}$$

The view angles, ψ_l, are computed by first tracing ν rays from each sub-surface and determining which surface each ray intersects first. This provides a list of surfaces "seen" by A_{ik} at ν angles from -90 to 90^o from the surface normal direction. The angles ψ_1 and ψ_2 that bound the view of each surface from sub-surface A_{ik} can be estimated from two adjacent rays, r_l and r_{l+1}, that encounter two different surfaces where

$$\psi = \frac{\psi_l + \psi_{l+1}}{2} \tag{2.13}$$

A simple example for three surfaces is shown in Figure 2.2, angles (ψ_a, ψ_b, and ψ_c) are calculated from rays originating from surface A_{1k}. The view factors from sub-surface A_{1k} to surfaces A_2 and A_3 can then be calculated as follows

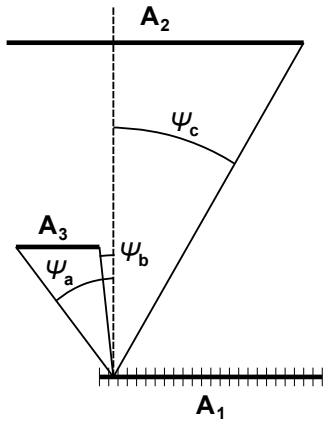

Figure 2.2: Angles between a sub-surface of A_1 and the visible areas of surfaces A_2 and A_3

$$F_{1k2} = \frac{\sin\psi_c - \sin\psi_b}{2}, \quad F_{1k3} = \frac{\sin\psi_b - \sin\psi_a}{2} \tag{2.14}$$

where the total view factors can be calculated using Equation 2.12.

With sufficiently small surface and ray angle discretization, errors with respect to the analytical view factor solution when considering simple geometries approach 1%. This algorithm also has the advantage of being easily parallelizable, where the view factor calculation for each surface can be allocated to a single thread or processor which greatly reduces computation time for a large number of surfaces.

2.3.2 Surface Modeling

The model considers three types of surfaces: i) burner panels, ii) insulating walls, and, iii) part surfaces. Below, we discuss the strategies for computing $Q_{net,i}$ in Equation 2.4 for each type of surface.

Burner Model Defining a model for the burner is necessary to find the net heat to the furnace provided by the burner. To simplify the view factor calculations in the radiosity model, the burner is approximated as a flat panel. In practice, radiant U-tubes are fired by natural gas to produce heat, where the natural gas enters at one end and combusts then exits at the opposite end as postcombustion exhaust. The burner model assumes an instantaneous and complete reaction at the entrance of the burner, with part of the heat of combustion being transferred to the furnace, and the remaining leaving the furnace as exhaust. The heat lost as exhaust is related to the blended heat capacity of the exit gases and temperature difference of inlet to burner temperature. For each individual burner, the burner model equation is thus:

$$\frac{\dot{m}_{fuel}\Delta H_{comb}}{1+AFR} = Q_{net,i} + \dot{m}_{fuel}C_{p,blended}\left(T_i - T_{in}\right) \tag{2.15}$$

In this equation $\dot{m}_{fuel}$ is the overall fuel mass flow rate, AFR is the air-to-fuel ratio, and T_{in} is the inlet temperature of the unreacted fuel. $C_{p,blended}$ is calculated as an averaged of the heat capacities of the exit gases assuming complete reaction. The temperature of the burner T_i is obtained via the burner surface temperature when solving the radiosity model (using $Q_{net,i}$ above as an input). We note that, typically, as the temperature of the burner rises, more heat exits as exhaust rather than enters the furnace.

Insulating Wall Model The model assumes that the refractory insulation is imperfect and leaks heat to the surroundings. To capture the dynamic temperature change of the furnace walls, a lumped capacitance model is considered. This is justified by the fact that the insulating material is typically thin, with a low mass. The energy balance for the wall incorporates the heat input from within the furnace as well as the heat lost to surroundings. We thus write:

$$\rho_{ins}V_{ins}C_{p,ins}\frac{dT_i}{dt} = Q_{net,i} - h_{air}A_i\left(T_i - T_{air}\right) \tag{2.16}$$

where T_i is the temperature of the wall, and h_{air} and T_{air} are properties of the air outside the furnace. The variables ρ_{ins}, V_{ins}, and $C_{p,ins}$ correspond to the density, volume, and heat capacity of the insulating wall.

Part Model We assume that a part is a solid, uniform body, which we model as a 2D rectangular domain. Following the solution of Equations 2.4-

2.5, the heat flow rates $Q_{net,i}$ at the part surfaces are used as to define the (Neumann-type) boundary conditions for this domain:

$$Q_{part,i} = -kA_i \frac{dT_i}{d\vec{n}} \tag{2.17}$$

where $\vec{n}$ is the direction normal to the heat input. For the purpose of the radiosity model, the temperature of the part surface is taken as the average temperature across the surface. The rectangular geometry considered for the parts allows us to use a two-dimensional Crank-Nicolson finite-difference scheme to compute the part temperature distribution. This consists of solving a linear system of the form:

$$\Gamma T^{n+1} = \Lambda T^n + \Phi \tag{2.18}$$

where matrices Γ and Λ are dependent on the thermal diffusivity, spatial discretization, and time step while the vector Φ holds boundary conditions. For computational simplicity, the thermal diffusivity of the steel, k, is held constant, and the spatial discretization as well as time steps are also held constant [Zhang et al., 2002]. This allows for the Γ and Λ matrices to be computed in the pre-simulation phase. After the radiosity model is solved at time step n, the heat input to the part is used by updating the Φ vector to find the temperature profile of the part at the next time step $(n+1)$. Time steps are chosen in conjuction with the view factor calculation to match the known part velocity through the furnace.

Fluid Model The blanket gas inside the furnace is assumed to be well mixed within each control volume (equivalently, the gas temperature inside the con-

trol volume is uniform), and the gas flow is assumed to be in one direction. We assume a uniform velocity profile in the cross section of the furnace. The change in temperature of the flowing fluid is found by accounting for the heat transferred by convection from the top and bottom furnace surfaces of a control volume to the fluid. As flow is in one direction, the heat gained one control volume w is transferred to the next control volume $w+1$. The heat exchange in control volume w is calculated via the enthalpy as a function of temperature of the fluid. The heat exchange in the next control volume $w+1$ is given by the addition of the heat from control volume w with the heat of convection from the ceiling and floor in control volume w. Then, the temperature of control volume $w+1$ can be found from the resulting enthalpy. Specifically:

$$Q_{w+1} = \sum_{i \in surfaces} h_{furn} A_i \left(T_i - T_w^{\infty}\right) + Q_w = \frac{H(T_w^{\infty})}{\dot{m}_{N_2}} \tag{2.19}$$

$$T_{w+1}^{\infty} = G(\frac{Q_{w+1}}{\dot{m}_{N_2}}) \tag{2.20}$$

This calculation is performed assuming nitrogen (with mass flow rate $\dot{m}_{N_2}$) is the only gas in the system. Enthalpy is determined as a function of temperature from a lookup table. The reverse calculation (determining temperature from enthalpy), is performed in the same manner. This is possible since nitrogen does not undergo any phase transformations and enthalpy is a monotonically increasing function of temperature. The fluid is assumed to enter the furnace at temperature T_{in} and exits only at the opposite end, i.e. there are no leaks within the furnace.

2.4 Solution Algorithm

In order to deal with the nonlinearities that arise from radiative heat transfer, as well as to account for the evolution of the insulating wall temperature, burner duties, and convective fluid temperatures, an explicit dual iterative scheme with fixed time step [Ramamurthy et al., 1995] is used to simulate the furnace.

The view factors for a set of pre-determined locations in the furnace are calculated prior to the simulation using the algorithm described in Section 2.3.1. The view factors are saved in a library that is loaded in the initialization step of the simulation.

The movement of the parts in the furnace is then approximated as a series of discrete events, consisting of each part moving between these predetermined locations. Part velocities are assumed to be defined by the speed of the conveyor belt. Thus, the distance that a part travels in one time step can be computed from the speed and the time step. This distance is then used to determine the new location of the part and the corresponding view factors. The choice of time step is driven by two factors: i) the time step must be small enough to capture meaningful changes in the part temperature distribution (as defined by the Crank-Nicolson scheme described in Section 2.3.2), and ii) the time step should be large enough so that it does not affect computational performance. The time step is bounded from above by the time interval between charging individual parts into the furnace.

Once a time step is chosen and the view factors are computed, the solution algorithm proceeds as follows:

1. Initialize system with view factors and initial furnace temperatures

2. Identify active parts by accounting for any parts that have been removed from the furnace and parts that have been newly introduced

3. Radiation Model (instantaneous)

   (a) Solve for convective temperature change given surface temperatures (Eq. 2.20)

   (b) Solve for radiosities from given surface temperatures (Eqs. 2.4 and 2.5)

   (c) Use radiosities to solve for new surface temperatures and heat inputs to insulating surfaces (Eqs. 2.4 and 2.5), which then are used to find new insulating surface temperatures (Eq. 2.16)

   (d) Repeat until change in temperature and radiosity between iterations meets specified tolerance

4. Use $Q_{net,i}$ for part surfaces as the boundary conditions for the part model in the Crank-Nicolson scheme (Eq. 2.17 and 2.18) and find temperature profile within each part

5. Advance parts to the next location, increase time by one time step and return to Step 2

For sufficiently small time steps and short part movements, the initial temperature conditions in Step 3 of the algorithm are typically near the value of the final condition, so a small number of iterations are needed to solve the radiation model. Figure 2.3 provides a flowchart of algorithm, showing the inner loop which is the radiation model solution algorithm.

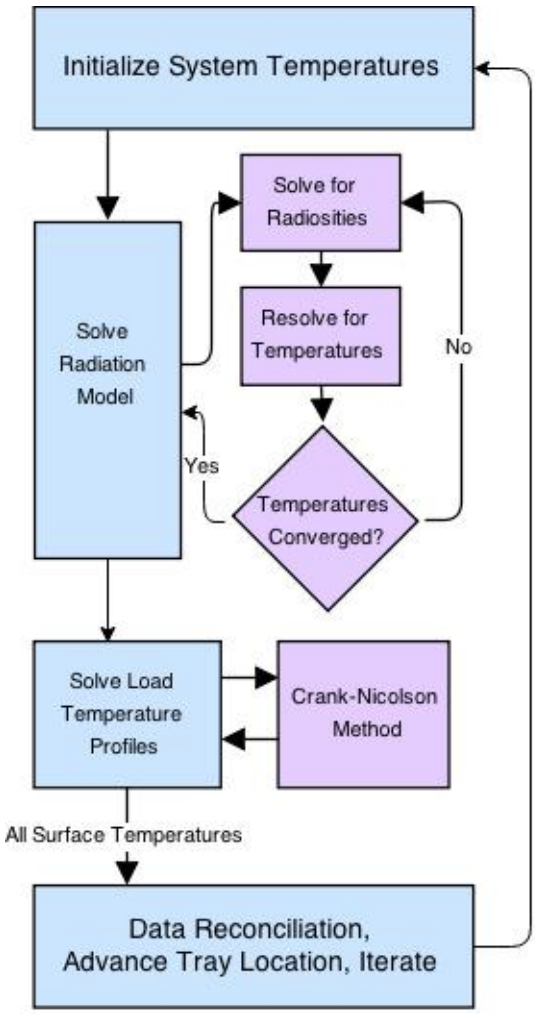

Figure 2.3: Dual-iterative solution algorithm for combined radiosity and temperature profile furnace model. Note the radiation model is instantaneous while the load model is time dependent.

Chapter 3

Model Case Studies

We consider here the simulation of a heat treating furnace from the plant mentioned in Section 2.1, with the purpose of validating our model as well as for assessing energy use in the existing physical system. In particular, we aim to identify how much heat is transferred to the parts during operation, as well as to identify the losses related to heat leak through the walls, to heat lost with the flue gas from the burners and with the blanket gas that circulates through the furnace.

We present three specific case studies in this section: the cold furnace startup and two production scenarios. The startup case showcases the ability of the model to account for the heating of the elements of the empty furnace. We also utilize this case to validate the numerical scheme. The production modes considered include, i) typical operation with low part throughput (which limits part-to-part interactions), and, ii) a high-throughput scenario, where we examine the effect of stronger part interactions and the tradeoffs involved in increasing the production rate.

The operational simulations both consider approximately 48 hours of simulation, which correspond to 82 parts in the first mode and 131 parts in the second mode. Each part remains inside the furnace for four hours total. Furnace temperature control is not considered, i.e. the burner fuel flow rates are held constant for the entire simulation. The simulations are carried out

using 64 control volumes and 130 total furnace surfaces. There are 32 ceiling burner panels and 16 floor burners.

3.1 Furnace Startup

The cold startup of the furnace involves considerable energy use without immediate production-related benefits, and, as such, should be carried out as quickly and efficiently as possible. Startup consists of bringing the furnace structure (including the insulating walls) to the high-temperature operating conditions.

The fuel flow is set to give burner duties of the ceiling burners at approximately $50kW$ and floor burners at $25kW$. In this startup case, no parts are present, limiting the simulation to only burner surfaces and refractory insulation.

The steady state solution is found by allowing the simulation continue until the change in net heat into the insulating walls computed between two consecutive time steps decreases past a given tolerance, in this case 0.1%. The time taken to reach steady state conditions is approximately eleven hours, which is in line with the expectations of typical operation as indicated by plant operators. To reach this steady state, 78 gigajoules of net energy input are required. The fuel flow rates per zone are the same in this case, and the resulting temperature of the furnace is approximately $1500K$. Figure 3.1 presents the distribution of heat at steady state after a cold startup. It is noticeable here that the majority of the heat exits with the burner exhaust and only 10% of the heat is lost through the walls; this is indicative of the fact that radiation is the dominant mode of heat transfer in the system.

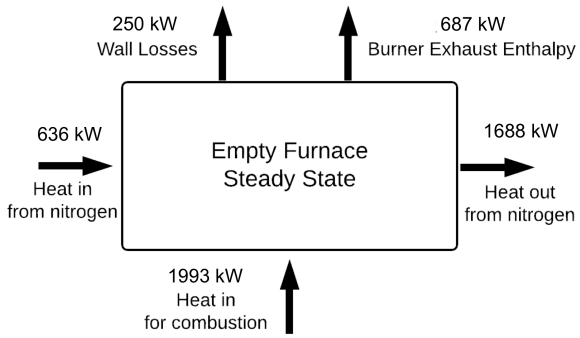

Figure 3.1: Heat distribution for empty furnace steady state. After cold startup, the majority of the heat exits as exhaust as well as with the flowing nitrogen. In this model, recuperation of heat from the exhaust flue gas and blanket nitrogen (entering at $400K$) are not considered.

3.2 Heat Treating Operation

Two heat treating scenarios are investigated, with both scenarios beginning with a warmed-up but empty furnace. The two scenarios consider different production modes, with the second scenario increasing the mass throughput of the process by fifty percent relative to the first. Given the steel part dimensions, the second operation mode corresponds to the maximum possible throughput, with the parts being almost in contact with each other as they pass through the furnace. Each scenario considers 48 hours of heat operation, which allows ample time for the furnace to adjust to steady state operating conditions for constant part input and output.

In both operation modes, the steel parts are within the furnace for four hours total. The goal in each case is to heat the steel parts to a minimum temperature of $1200K$ using the same amount of fuel distributed in different

manners across the furnace. The secondary goal is to maintain a relatively uniform temperature distribution within the part.

3.2.1 Low Throughput Operation

The first operating mode is in line with the current mode of operation of the plant. In this mode, there are at most eight parts within the furnace at a given time, corresponding to a steel throughput of four tons per hour. New parts are charged to the furnace at thirty minute intervals. Following suggestions from operators, the zone fuel flow rates are chosen so that zone 1 is approximately at $1000K$ and zones 2-4 are at a higher temperature, for this we choose $1200 - 1250K$. The overall heat input rate is $1.5MW$. The heat inputs per zone are $550kW$, $450kW$, $300kW$, and $200kW$. Forty-eight hours of simulation are considered, corresponding to a production run of 82 parts.

A map of the temperature profile within the domain of the furnace during steady state operation (i.e. not the "head" or "tail" of the batch) is shown in Figure 3.2. This figure shows the temperature of the furance walls are at a maximum in zone 3, which is to be expected due to both maximized sightlines from the furnace burners as well as the parts being near exit temperature at this point.

Considering the exit conditions for each part, we note that the system requires more than one full cycle of parts (where each eight part subset is one cycle) to approach "steady state," or consistent input-output behavior. Upon reaching the (periodic) steady state, the total energy transferred to each part is approximately $916MJ$. After the twelfth part, corresponding to the sixth hour of operation, the system reaches steady state for constant throughput. The maximum energy is $956MJ$ for part number 82 and the minimum is $838MJ$

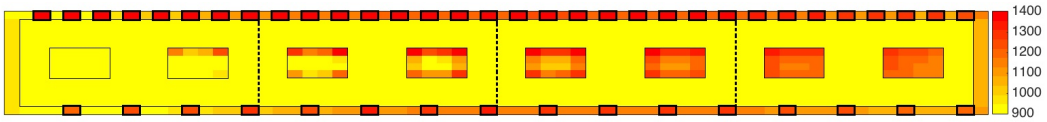

Figure 3.2: Heat map of the furnace during steady state (constant input-output) operation in the low throughput mode. The temperature range is $900K - 1400K$ to highlight temperature differences at the upper end of the spectrum. To restrict the temperature range, we use "clipping," and all temperatures lower than $900K$ are shown in the hue corresponding to $900K$. The temperatures of the leftmost steel part as well as the furnace gas are below the $900K$ threshold. Burners are highlighted with bold line, and parts are highlighted with a thin line. The granularity of the part temperature profile is increased for this explanatory figure, but these results do not vary significantly (i.e., are within $10K$) from those obtained using the detailed model described in the rest of the thesis.

for part number 1 as seen in Figure 3.3. The average (computed as an average temperature over the discretized 2D domain) and minimum exit temperatures for each part are also considered. The average temperature of a part during steady state operation is $1283K$, while the minimum part temperature during steady state operation is $1234K$. It is notable that the difference between the average and minimum temperatures is relatively small. The increase in total heat per part and in part temperature as more parts are processed can be attributed to the increase in thermal mass of the furnace as the production run proceeds. In this context, three sub-periods of operation can be delineated:

- *Ramp up* corresponds to parts entering an empty furnace, and lasts until the steady-state furnace loading is reached.
- *Steady state* is the sub-period of constant part input-output.

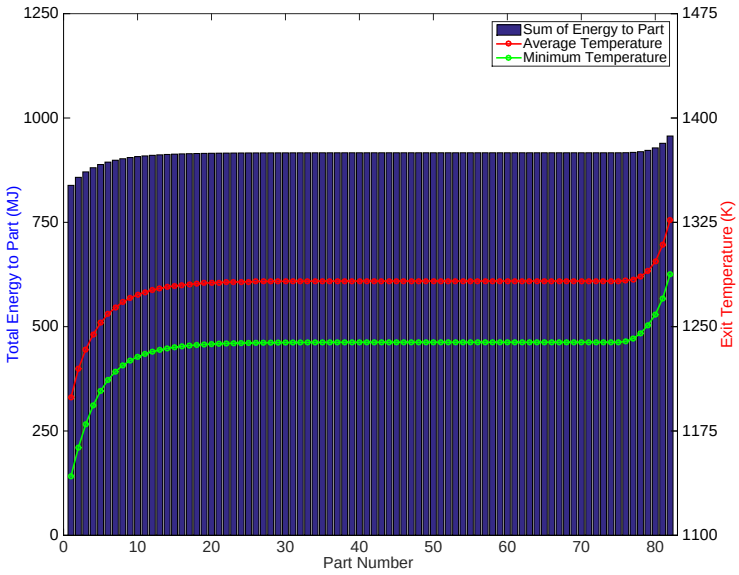

Figure 3.3: Part exit conditions for 82 parts in the first operational mode (low throughput).

- *Ramp down* occurs as the furnace begins to empty, and lasts until the last part exits the furnace.

Through ramp up and ramp down, the exit temperatures of the parts reflect the total energy each part receives in the furnace, and will thus vary due to changes in view factors and the nature of the interactions between the parts and the furnace elements, and between the parts themselves.

3.2.2 High Throughput Operation

In this scenario, a part is charged to the furnace as soon as there is enough free space. This allows for 12 parts to be within the furnace at any

given time. Thus, 131 parts can be processed in the same 48 hour operating time considered in the previous case. The fuel flow rates to the burners in each zone were adjusted so that the exit minimum temperature of the parts was the same as in the low throughput operation mode. The *total* energy input to the furnace was kept at the same level as in the previous case, i.e., $1.5MW$. In this case, the heat inputs per zone are $498kW$, $448kW$, $299kW$, and $249kW$, respectively.

The exit conditions for this scenario are shown in Figure 3.4. During the steady-state sub-period, the each part receives $968MJ$ and the average part exit temperature is $1338K$, which is approximately $50K$ greater than in the first operation mode. The minimum part exit temperature for this sub-period is $1223K$, which is within $10K$ of the previous case. As in the previous case, the average energy acquired by the parts increases during the steady state period (compared to start-up) due to thermal inertia of the furnace.

In comparing the low throughput and high throughput operation scenarios, one must consider both the impact of *increased product mass* and the effect of the corresponding *increase in furnace thermal inertia*. Conventionally, increasing the amount of material to be heated with constant heat input should result in lower temperatures, since the energy input is distributed to a larger mass. However, up to a certain point, the rise in thermal inertia of the overall furnace from an increase in mass outweighs the effect of increased mass. In essence, more heat is absorbed by the parts, due to the fact that there are more parts. This can be seen as a result of radiation heat transfer being the dominant form of heat transfer.

This is not to say that increasing the steel mass in the furnace indefinitely will result in greater furnace temperatures; such would violate the energy

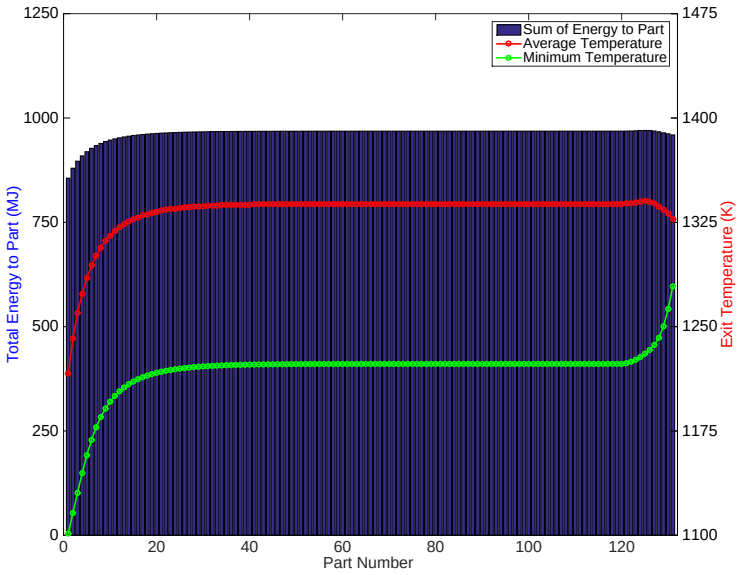

Figure 3.4: Part exit conditions for 131 parts in the second operational mode (high throughput).

balance. The model does predict a decrease in temperatures after increasing the mass throughput past a given threshold.

3.2.3 Comparison of Operation Modes

The efficiency of the system is examined by considering the heat distribution across the furnace during *steady state* operation. It is expected that increasing the metal throughput would increase the energy efficiency of operation. Table 3.1 confirms this postulation.

The data in Table 3.1 are computed by aggregating one complete cycle (i.e., examining the heating conditions for one part during its four hours of residence in the furnace). Note that the total heat input from the burners is

Heat Sources and Sinks	Operation Mode 1	Operation Mode 2
Heat Input from Burner	3.18	2.27
Heat to Parts	1	1
Heat Out of Exhaust	1.23	0.71
Heat to Flowing Nitrogen	0.89	0.52
Heat Through Insulation	0.06	0.04

Table 3.1: Normalized heat distribution over one period of furnace operation, for both operation modes. This table shows the required heat input to the burner for every kilowatt to the part surface, as well as the distribution of energy to other heat sinks in the furnace.

held constant.

We define the fuel heat-to-load efficiency as the ratio of the total energy absorbed by the parts to the total the energy input from combustion to the system. The efficiency in the first operating mode is 31%, and the second operation mode has efficiency of 44%. These efficiencies are in line with the 20% to 40% gross fuel to load efficiencies cited in the literature [Thekdi, 2010].

In the first operation mode, the amount of heat lost with the burner exhaust exceeds the energy gained by the steel parts. Heat leak through the walls is comparatively modest, accounting for approximately 2% of the heat input.

Figures 3.5(a) and 3.5(b) show the heat input and average temperature as a function of time for a part during the steady state sub-period. In both cases, the amount of heat transferred to the parts decreases with time and position in the furnace. A significant fraction of heat transfer occurs in the first zone, since here the driving force (largely determined by the temperature difference between the part surface and the burner surfaces) is the greatest. A key difference in the rate of heat input to the parts is that in the first

operating mode, its value approaches zero steadily in time, whereas in the second operating mode, there is a large drop near the end of the time a part spends in the furnace. This latter effect is due to the close proximity of a part to the precedent one (i.e., the one located ahead in the furnace), and the influence of that part on the rate of heat input. We believe that the large gap between the average and minimum temperatures in the second operating mode (Figure 3.4) is in part due to this step change in heat-to-part.

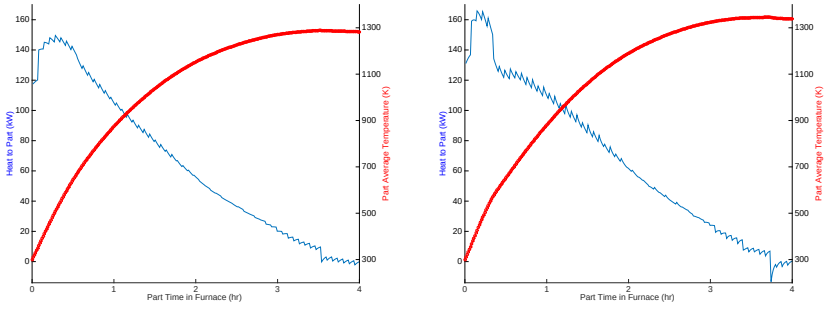

(a) Operation Mode 1 (b) Operation Mode 2

Figure 3.5: Time profile of a steady state part as passes through the furnace. The two plots are largely similar and show that the majority of heating to the part is done in the beginning of the furnace. A key difference is the drop to net negative heat flux, which occurs earlier and less impactfully in the first mode than the second.

Differences between the two operating modes are also seen in terms of the zone temperatures of the furnace (Figures 3.6(a) and 3.6(b)). Note that for the first operation mode, the fuel flow rates were computed to give a desired zone temperature profile as suggested by industry operators. In the second case, the flow rates of fuel to the burners were empirically redistributed to obtain the same exit minimum temperature as in the first case. This required decreasing the fuel flow rate in the first zone of the furnace and increasing

the fuel flow rates in the last two zones. The zone temperatures in operation mode 2 are greater than in operation mode 1. In both cases, the burner fuel flow rates decrease from zone 1 (part feed point) to zone 4 (furnace exit). This accounts for the fact that zone 1 receives the cold parts and thus has the highest energy demand (and the lowest temperature). The subsequent zones do not require heat input rates as high as zone 1 to reach desired temperature ranges because in the respective locations the parts are warmer and the rate of heat absorbtion diminishes.

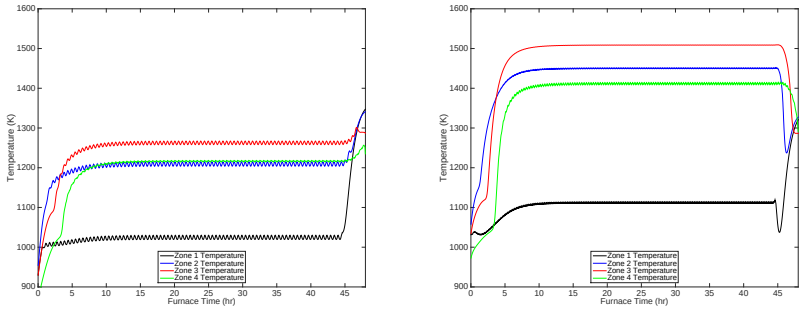

(a) Operation Mode 1 (b) Operation Mode 2

Figure 3.6: Furnace zone temperatures as a function of time.

The increase in fuel-to-part efficiency that is associated with increased throughput suggests that operating the furnace in a high throughput manner is more efficient. However, this increase in efficiency is obtained at the cost of a higher variability in the temperature distribution within the parts. These results match the conclusions published by Chen et al. [2005]. Chen et al. [2005] also discussed the necessity of minimizing part temperature spread in order to ensure high quality downstream processing in the oil quench and tempering furnace.

3.3 Computational Performance

Using an error tolerance of 0.1% in the temperature and radiosity, about one and a half hours of CPU time (using a personal laptop running Windows 8 with a 3.3GhZ Intel Core i7 Processor and 8GB RAM) is required to simulate 48 hours of system operation. While other models in literature, such as Steinboeck et al. [2010] and Kang et al. [2007] report better computational performance, we believe that our results are very reasonable given the increased detail of the model.

Chapter 4

Control and Real Time Optimization

4.1 Furnace Control and Tuning

With a detailed model of the furnace system, implementing feedback control of the furnace to mirror operation in the plant is desired. In the previous modeling section, constant fuel flow to the burners was considered. In actuality, the furnace is operated by manipulating (i.e. changing in time) the fuel flow rates to the burners to control furnace temperature. Control of the furnace temperature is distributed across control zones within the furnace where burners in a control zone work together to control the temperature of that zone. Each control zone is operated independently of other zones. Note that long range radiation interactions are present such that adjustments to the fuel flow to the burners in one zone will cause residual effects on other zones due to radiative heat transfer. Also, parts entering the furnace at ambient temperature cause a significant disturbance in the temperature of the first zone.

In the model, the controlled variable is the temperature of the insulating wall subsurface in the center of each control zone (see Figure 2.1, where the circled subsurface is the controlled surface). In the real furnace, there is a thermocouple at this location which provides temperature readings. Due to the nature of surface-to-surface radiative heat transfer in the system, it is necessary that the controlled variable be a surface, rather than the gas temperature. The

gas temperature within the furnace is much lower than the wall temperatures (see the heat map in Figure 3.2) and is not an appropriate indication of the state of the furnace.

4.1.1 Improved Burner Model

The burner model used in the previous section was not sufficient when considering feedback control of the system. The previous burner model was appropriate for steady state simulations since the model did not include time variations of the fuel flow rates. When considering feedback control, the controller varies the flow rate of fuel to the burner. This is done to modulate the heat input to the furnace and thus control the furnace temperature. The issue is that in the previous constant fuel flow rate case, a steady state approximation was made on the burner temperature. While burner temperature is a strong function of the mass flow rate of fuel, in the previous cases, the burner temperature did not vary greatly since the fuel flow rate was held constant. As a result, the model used thus far does not properly account for thermal interactions when the fuel flow rate control to the burners changes. Specifically, the temperature of the burner walls changes immediately after a step change in the fuel flow rate, since the thermal intertia of the burner walls is not taken into account. As a result, a new burner model is developed which takes into account the time dependent temperature dynamics of the burner walls.

We will use a burner model based on the work of Niederer et al. [2014]. In this model, the dynamics of the burner walls are included, and they are approximated with a lumped capacitance model. The model considers two gases, the inlet gas (IG) to the burner, containing $[CH_4, O_2, N_2] \in IG$, and outlet gas (OG), containing $[CO_2, H_2O, O_2, N_2] \in OG$. The IG and OG cap-

ture the components involved in the combustion of methane in air, governed by the equation $CH_4 + 2O_2 \rightarrow CO_2 + 2H_2O$, where N_2 is an inert gas which does not contribute to the reaction. We assume fuel-lean operation, such that all methane is consumed.

The heat to the burner provided by the inlet gases is the heat of combustion less the specific enthalpy of the gases, given by the following equation [Niederer et al., 2014]:

$$Q_{IG} = \sum_{\xi \in IG} \frac{\dot{m}_\xi}{MW_\xi} (\Delta H_{comb,\xi} - h^{Ent}(\xi, T_{IG})) \tag{4.1}$$

where $\dot{m}_\xi$ is the mass flow rate, MW_ξ is the molecular weight, $\Delta H_{comb,\xi}$ is the heat of combustion, and $h^{Ent}(\xi, T_{IG})$ is the specific enthalpy, all for gas $\xi \in IG$. In this equation, it is assumed the temperature of the inlet gases, T_{IG} is known a priori.

Similarly, the heat out the exhaust in the outlet gases OG, is given by the following equation [Niederer et al., 2014]:

$$Q_{OG} = \sum_{\eta \in OG} \frac{\dot{m}_\eta}{MW_\eta} (\Delta H_{comb,\eta} - h^{Ent}(\eta, T_{OG})) \tag{4.2}$$

which is an equivalent equation to Equation 4.1 for gases $\eta \in OG$. We assume the appropriate amount of CO_2 and H_2O were formed stoichiometrically after all CH_4 is consumed. T_{OG} is assumed to be known a priori as with T_{IG}, which constitutes a major assumption in the model.

The heat that leaves the burner is given by the difference between Q_{IG} and Q_{OG}, but an additional term for the heat buildup of the burner wall is

included. We use a lumped capacitance approximation of the tube wall, and the heat balance around the wall is then given in the following equation:

$$Q_{burner} = Q_{IG} - Q_{OG} - V_{burner}\rho_{burner}C_{p,burner}\frac{dT_{burner}}{dt} \tag{4.3}$$

where the $_{burner}$ subscript denotes burner characteristics, i.e. density, heat capacity, and temperature. The change in burner temperature with time is given by the radiation part of the model (see Section 2.3).

These changes to the burner model allow for simulations of the closed-loop control of the system to be performed. We note that modeling radiant tube burners is a research topic in its own right [Mochida et al., 1997, Tiwari et al., 2005], and the assumptions made in this model are necessary in order to obtain a simple input/output burner model that is easily tractable in computational simulations.

4.1.2 Controller Tuning

We begin by implementing a linear, proportional-integral control system to vary the flowrate of fuel to the burners. Operators indicated that in the physical facility, the fuel flow rate is regulated by means of a butterfly valve. The burners operate in two modes; low-fire and high-fire. In modeling the burner, the low-fire mode indicates a minimum allowed fuel flow rate, that is, the butterfly valve does not fully close. Any fuel flows greater than the minimum are designated as high-fire operation. We also designate a maximum fuel flow rate to capture situations when the butterfly is fully open (i.e. saturated).

Tuning of the controllers was performed on an empty furnace and

Ziegler-Nichols tuning rules are employed. The aggressive nature of Ziegler-Nichols tuning [Seborg et al., 2004] is potentially appropriate to reject disturbances associated with part input/output operation. Each of the zone temperature controllers are initially tuned independently of one another, but due to similarities in the ultimate gain (0.1) and ultimate period (330s) across the zones, it was decided to use the same values for the controller gain, $K_p = 0.05\frac{kg/s}{K}$, and integral time constant, $\tau_i = 275s$, in each zone.

4.1.3 Heuristic Results

In practice, furnace operation is largely based on operator experience. Temperatures controller set points are decided based on past experience and heuristic process knowledge rather than using a comprehensive physical understanding of furnace phenomena. In this section, we analyze the operation of the furnace based on these heuristic principles, and obtain a baseline for energy consumption.

The temperature set points used in this simulation are $1000K$, $1100K$, $1150K$, and $1200K$. These were chosen from temperature ranges provided by the operators of the industrial plant. Importantly, zone 1 operates at a lower temperature than the rest of the furnace, while from zone 2 to 4 temperature increases in each consecutive zone. The simulation considers the heating of 40 steel parts, with eight parts being within the furnace at any given time, corresponding to approximately 25 hours of operation. There is no explicit goal in part exit quality or temperature; this simulation is used to examine what is occuring within the furnace given heuristic operation and to provide a baseline energy consumption.

The closed-loop furnace simulation illustrates that the proposed control

system case maintains the zone temperatures with minimal variations (within $8K$ of the set point), as shown by the top row of plots in Figure 4.1. The inputs (fuel flow to the zones) are shown in the bottom row of plots of Figure 4.1. An important feature of the zone temperature results is their oscillating nature. The oscillations in zone 1 are nearly pure sinusoids, while the temperatures in the later zones fluctuate at other frequencies. The variations in temperature in zone 1 can be attributed to the (known) disturbance of a cold part entering the furnace every 30 minutes, which is the dominating harmonic. As a new part at ambient temperature enters zone 1, it draws heat from the furnace surroundings. To account for this, the fuel flow in zone 1 is set to the maximum, saturated position. An upper limit of the fuel flow rate prevents the controller from reaching the magnitude necessary to better reject this disturbance.

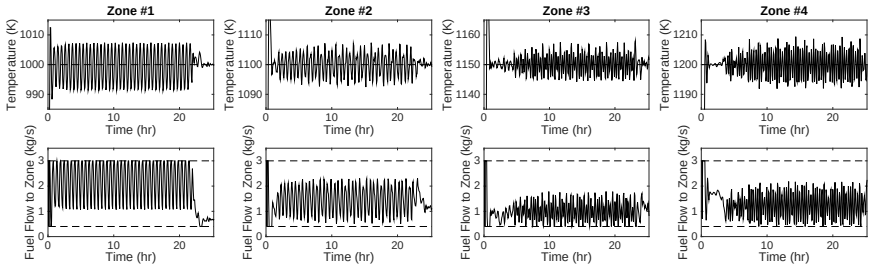

Figure 4.1: Zone temperatures (controlled variable) and total fuel flow to zones (manupulated input) for the heuristic temperature set points $1000K$, $1100K$, $1150K$, and $1200K$. Zone 1 features a sinusoidal variation in both the temperature and fuel flow rates, later zones show additional oscillation frequencies.

Variations in temperatures in other zones can be attributed to the same cause, but with a less pronounced effect from the input of parts. The parts entering later zones are warmer than ambient temperature, so the effect of the part entering a later zones is less significant. An aspect to note is that while

control of the furnace is done individually per zone, there are zone-to-zone interactions from long distance radiation effects.

When examining the exit conditions (Figure 4.2) of the parts as in Section 3.2, we immediately notice three results. First, fewer parts should be processed for the minimum part exit temperature to reach the steady state value of $1182K$. Second, the parts at the beginning and end of the batch have lower variance in total energy absorbed and in temperature than the constant fuel case (see Figure 3.3). Finally, both the average temperature and total energy at exit are "noisy" from part to part. We attribute the faster settling time due to feedback control which maintains a consistent furnace temperature even as the thermal mass of the furnace changes. The "noise" is a result of the temperature of the parts nearing the burner temperature at the exit of the furnace. As these temperatures approach one another, the driving force is minimal and small temperature swings can change the sign of the heat flux of the part. The average temperature is $1235K$ and the average exit energy is $1005MJ$ per part.

Finally, we examine the heat input and temperature of the 20th part (steady state conditions reached by this point) as a function of time (and thus position) within the furnace (Figure 4.3). Recall in the previous case, Section 3.2.3 the heat to the part was a relatively smooth, decaying curve (Figure 3.5), a result of the constant fuel input to burners. In this case, the heat to the part features oscillations with a general decaying trend, which is due to the presence of feedback in temperature control in the furnace, as the oscillations are not seen when considering constant fuel input (Figure 3.5(a)).

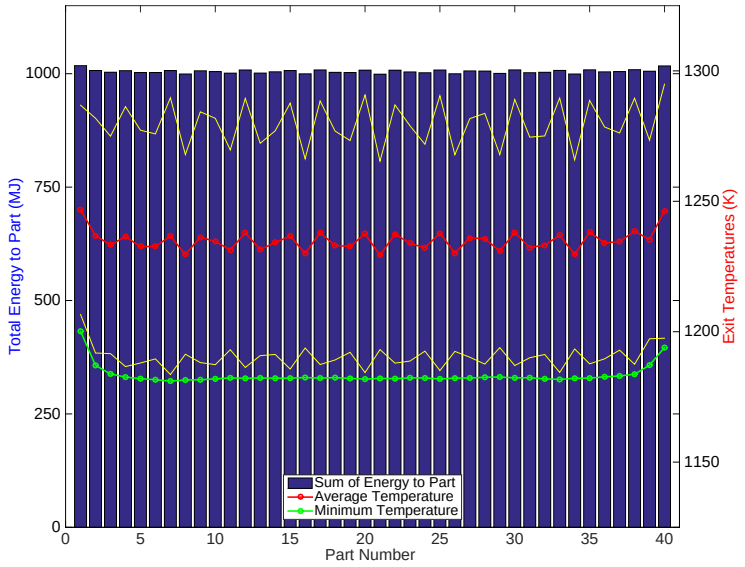

Figure 4.2: Part exit conditions for 40 parts in the heuristic operation. The yellow lines show the standard deviation around the average part temperature. The "noise" in the total exit energy and average temperature is due to the parts being at a greater temperature than the zone 4. The temperatures being near one another is the cause of "noise" to these values.

4.2 Real Time Optimization

The previous section provides insight into the furnace dynamics. The real advantage of the model, however, is the ability to predict furnace heat distribution and part exit properties, and to find the best (i.e., most energy efficient) manner to operate the furnace. To this end, we propose using real time optimization [Seborg et al., 2004] of the process to choose optimal zone temperature set points. For the case of a direct-fired reheating furnace, Yang and Lu [1988] have shown the benefits of optimization to achieve energy savings and controlling part temperature profiles in a direct-fired reheating furnace.

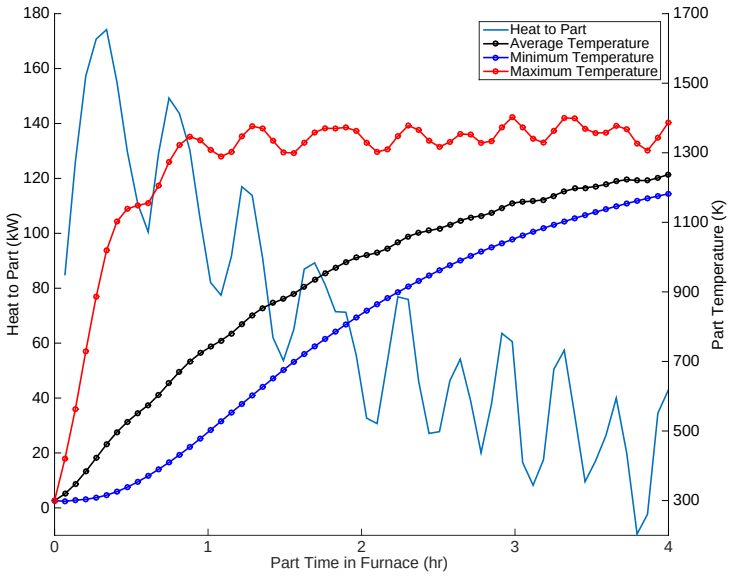

Figure 4.3: Heat input to the part and temperatures for part number 20 with time in the furnace (and thus position). Note the oscillatory decaying heating profile. This is a result of the fuel input to burners varying to control temperature. The heat to the part is more dependent on the heat input to the system rather than the temperature of the zone.

However, there are no results in the open literature concerning the optimization of the operation of *indirect-fired* furnaces.

The primary goal of the process is to heat steel parts to a certain temperature threshold with minimal temperature differences within the part. While the plant has successfully performed this for decades using operator knowledge, the benefit of the model is the added capability of predicting exit temperatures and minimizing energy consumption. In other words, we are now focusing on the question, "Can energy use in the plant be minimized *without* compromising product quality?" To address this question, we generate a non-

linear program which uses zone temperature set points, u, as a variable to achieve minimal energy usage while maintaining certain part quality. Specifically, we consider the following optimization problem:

$$\begin{aligned} \underset{u}{\text{minimize}} \quad & Energy\,Input\,per\,Part = f(u) \\ \text{subject to} \quad & Process\,Model \\ & Temperature\,Set\,Point\,Limits \\ & Minimum\,Part\,Temperature\,Threshold = h_1(u) \\ & Maximum\,Part\,Temperature\,Standard\,Deviation = h_2(u) \end{aligned} \tag{4.4}$$

The model inputs are the zone temperature set points for each individual zone. The selected model outputs are total heat input the furnace per part, minimum part exit temperature, average part exit temperature, and temperature standard deviation at exit. The total heat input to the system per part is what we aim to minimize. The minimum part temperature defines a desired temperature threshold for the parts at exit. The average part temperature and standard deviation of temperature are used to define temperature variations across the part, where this variation is aimed to be minimized. We use a metric from Badgwell et al. [1995], who defined standard deviation in temperature divided by average temperature as a quality measure for controlling silicon wafer temperatures. Given the similarities of the nature of the wafer heating process and the heat treat furnace, the same metric is used here.

Solving the nonlinear program is challenging due to the complexities of the model (Section 2.3). In its current form, the model is procedural due to the way that radiative heat transfer interactions are calculated. This is a

considerable impediment in the calculation of gradients, which are required by modern optimization solvers.

Instead, we will use response surface surrogate models, (for an overview on *Response Surface Methodology*, see Myers et al. [2009]). Surrogate models are a method of approximating black or grey box simulations of complex models. Sample points in the input space are used to calculate the corresponding output values of the corresponding original model, and a simplified system of algebraic (or differential) equations relating the outputs as a function of the inputs can be formulated. This "surrogate" model can then be used to approximate the true model for fast simulation and optimization purposes. The accuracy of the surrogate model depends on the choice of the functional form of the equations, as well as the number of data points used to fit the equation parameters (model). For any model output z, the surrogate model approximates z as $\hat{z}$, which is a sum of basis functions as a function of inputs $X_j(u)$, as shown below:

$$\hat{z} = \sum_{j \in B} \beta_j X_j(u) \tag{4.5}$$

where β_j are coefficients (e.g. found via ordinary least-squares regression).

$$\min_{\beta} (z - \sum_{j \in B} \beta_j X_j(u))^2 \tag{4.6}$$

Basis functions, $X_j(u)$, are functions of the inputs, i.e. polynomial, exponential, or products between different inputs. By deciding the form of the basis functions a priori, this becomes a linear regression on the coefficents β_j. This

formulation gives an approximation of the outputs as an algebraic function of the inputs.

Our method of using surrogate models to find the optimal inputs is based on the work by Cozad et al. [2014]. In Cozad et al. [2014], an extensive surrogate model generation algorithm is developed and used to generate an algebraic surrogate model of any system from a set of system input and output data. The algorithm automatically chooses the proper basis functions and fits them to the given input/output space, using Akaike Information Criterion (AIC) [Akaike, 1987] to decide the number of basis functions needed to accurately model the system. AIC is used to evaluate increased model accuracy with each added basis function. We use many of the concepts introced by Cozad et al. [2014] in this work, but we do not rely on the actual software. One reason is the complex basis function combinations automatically used by their software are not necessary, as we already have a good understanding of which basis functions are physically applicable to our system, as discussed below.

We begin the development of the surrogate model of the furnace by sampling an initial input space. We then build a surrogate model with predetermined basis functions. The surrogate model is used for optimization, and the optimal point is added to the input/output set. We then reidentify the parameters of the surrogate model and continue the process to achieve higher fidelity results near the optimal point. We use an iterative approach, as follows:

1. Use Latin Hypercube Sampling to build an input space given upper and lower bounds of the inputs (temperature set points) and simulate the full model with these inputs to give corresponding outputs

2. Develop a surrogate model using *LASSO* [Tibshirani, 1996] for least squares regression. The basis functions chosen are linear (T), fourth order polynomial (T^4), and product pairs between two inputs (T_1T_2, T_1T_3, etc.). These basis functions are chosen due to physical characteristics of the system (heat transfer via convection and radiation) and the necessity to relate the temperatures in different zoness to each other. Using consistent basis functions for all outputs simplifies the implementation.

3. Use the algebraic surrogate models of the outputs in a nonlinear program (Equation 4.4) to find the optimal temperature set points given the objective and constraints. If the set points found by the optimization routine are "close" (Euclidean distance is relatively small, in our case we choose 10 which corresponds to all temperatures being within at least $5K$ of one another) to any other inputs already in the input set, stop. If not, solve for the outputs from the optimal inputs, and add the input/output pair to the set, and return to the previous step (i.e. improve the model).

The iterative algorithm stops when the found optimal input is already in or close to the input solution space. This methodology benefits from increasing model fidelity near the optimal solution.

This formulation is advantageous since it is systematic and can be applicable to different optimization schemes within the framework of this furnace modeling (such as finding optimal fuel flow rate for constant fuel operation). Depending on how large the initial sample space is, the optimal solution can be found in just a few iterations.

In developing the surrogate models, we consider only the constant part input/output region, so the beginning and end of each batch of the simulation are not used to define model output. To ignore dynamics of reaching a new steady state, the model allows for one and a half cycles (each cycle is eight parts due to eight parts being within the furnace at maximum) to be processed before recording part condition outputs for the surrogate model formulation. The output conditions are averaged over 12 parts during the steady state constant part input/output.

4.2.1 Surrogate Model Results

Using the methodology described in the previous section, the system was simulated to generate a surrogate model of the outputs and perform real time optimization. An issue in application of the algorithm is in creating the initial sample space which will lead the parameter estimation routine to an accurate optimal point with limited iterations. Since computational cost was not a factor, 501 initial Latin Hypercube Samples were taken across the input space. The large number of initial samples defines a detailed input/output space. From this, we can generate response surfaces of all outputs as a function of the temeprature set points, as shown in Table 4.1. Plots of the response surface for the part standard deviation are shown in Figure 4.4. The input space is 4-dimensional, so two values are held constant for each subplot. These plots suggest that in order to minimize standard deviation, zone 2 and zone 4 must be at $800K$ (standard deviation is a strong function of the zone 2 and zone 4 set points). When the temperature in those zones are set at $800K$, the temperature set point of zone 1 and 3 do not have a strong influence on the predicted standard deviation.

Output $\tilde{z}$	β_1	β_2	β_3	β_4	β_5	β_6	β_7
Min Temp	0.1334	0.2206	0.3527	0.3761	-0.0645	0.0590	0.2499
Avg Temp	0.1045	0.1892	0.2891	0.3944	-0.0639	0.0757	0.2160
E_{in}/Part	0.1441	0.1924	0.2595	0.3688	-0.0900	0.0733	0.1931
STDEV	-0.0956	-0.1503	-0.1221	0.3086	0.0307	-0.0148	-0.0125
	β_8	β_9	β_{10}	β_{11}	β_{12}	β_{13}	β_{14}
Min Temp	0.1808	0.0329	0.0631	-0.1987	-0.0408	-0.2509	-0.0220
Avg Temp	0.2567	-0.0372	-0.0807	-0.2575	0	-0.1707	-0.0061
E_{in}/Part	0.2238	-0.0392	-0.0758	-0.2466	0.0112	-0.1541	0.0321
STDEV	0.2321	-0.1172	-0.2300	-0.2331	0.0706	0.1529	-0.0714

Table 4.1: β coefficients for the surrogate models of the outputs as a function of inputs. The form of the algebraic surrogate model for all outputs is: $\tilde{z} = \beta_1\tilde{T}_1 + \beta_2\tilde{T}_2 + \beta_3\tilde{T}_3 + \beta_4\tilde{T}_4 + \beta_5\tilde{T}_1^4 + \beta_6\tilde{T}_2^4 + \beta_7\tilde{T}_3^4 + \beta_8\tilde{T}_4^4 + \beta_9\tilde{T}_1\tilde{T}_4 + \beta_{10}\tilde{T}_2\tilde{T}_4 + \beta_{11}\tilde{T}_3\tilde{T}_4 + \beta_{12}\tilde{T}_1\tilde{T}_3 + \beta_{13}\tilde{T}_2\tilde{T}_3 + \beta_{14}\tilde{T}_1\tilde{T}_2$. In this formulation, $\tilde{z}$ is the output, and $\tilde{T}_\psi$, $\psi \in [1, 4]$ are the temperature set points of each individual zone ψ. The *tilde* corresponds to the mean centering and scaling transformation of the variables, i.e. $\tilde{\xi} = (\xi - \xi_{mean})/|\xi_{max}|$, where ξ is the raw variable, ξ_{mean} is the average value of ξ in the dataset, and $|\xi_{max}|$ is the greatest value of ξ, used to scale the data between 0 and 1.

When searching for the optimal set points, the objective is to minimize the amount of energy input to the system from the burners per part heated. The constraints for part exit conditions are a minimum temperature of $1100K$ and a standard deviation divided by the mean temperature less than 0.03. Input constraints on the zone temperatures are a minimum of $800K$ and maximum of $1200K$ for all zones. After building the initial input space, six iterations of the scheme shown in Section 4.2 are needed to converge on the optimal solution. The optimal solution found are the set points $[967K, 800K, 1200K, 800K]$. We used the nonlinear solver IPOPT [Wächter and Biegler, 2006] to find the optimal set points.

The simulation with optimal temperature set points is performed with

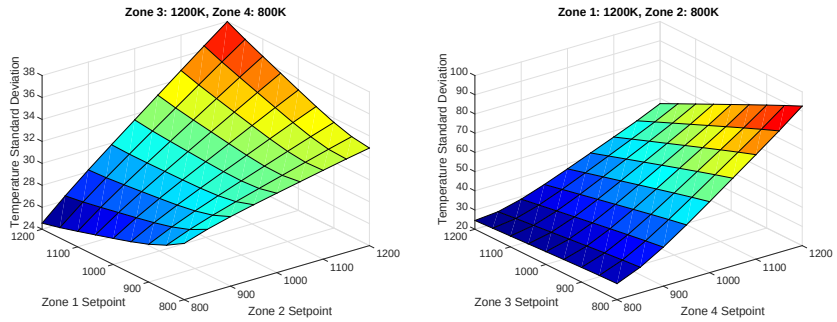

(a) Response Surface 1 (b) Response Surface 2

Figure 4.4: Response surfaces for the standard deviation of temperature. The model has 4 inputs, i.e. the temperature set points in each of 4 zones. Two plots are shown, holding two temperatures constant. These plots show minimal temperature deviations when zones 2 and 4 are at their minimum value ($800K$). The standard deviation does not strongly depend on zone 1 nor 3.

eight parts within the furnace at a given time, processing 40 parts for four hours each, resulting in approximately 25 hours of furnace operation. The resulting zone temperatures and fuel inputs are shown in Figure 4.5. We see here that zones 1 and 3 are able to reach their set points, but zones 2 and 4 do not. Zones 2 and 4 are set to the minimum allowable temperature ($800K$), but even with the minimum fuel input, the result is well above the set point. This partially due to the part temperature when they reach these zones. At zone 4, the parts are near exit temperature, $1100K$. The hot parts interact with furnace walls and since the fuel input is at a minimum, this shows the minimum temperature the zone will be at. Zone 2 suffers from similar effects, even though the parts are not as warm at that point. It is likely that the combined heat from radiation from zones 1 and 3 is influencing zone 2 and raising the temperature. The fuel flow rates to zones 1 and 3 are in the middle to upper range of allowable input; consequently there is a significant amount

of heat entering the system in these zones, which can then leak to the other zones.

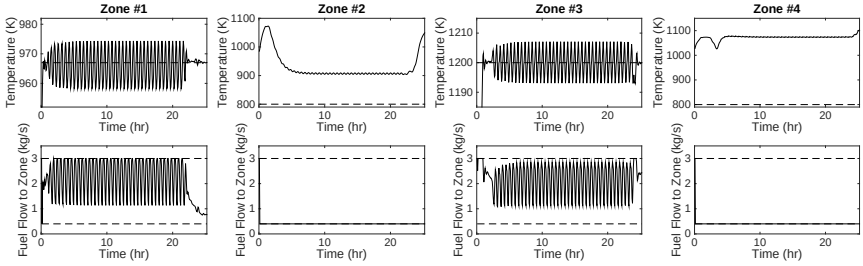

Figure 4.5: Zone temperatures (controlled variable) and total fuel flow to zones (manipulated input) for the optimal temperature set points $967K$, $800K$, $1200K$, and $800K$. Zones 3 and 4 are unable to reach the desired set point even with minimal fuel input to the system.

Next, we look at the exit conditions of the steel parts, as shown in Figure 4.6. We see here that the system quickly stabilizes to the steady state values, where the total energy per part is 907 megajoules, the average part temperature is $1144K$, and the minimum part temperature is $1095K$. We note that there is an offset in minimum temperature from the desired value of $1100K$, owing to the fact that the surrogate model has a small inaccuracy in predicting the temperature. This is likely due to the broad input space being used in developing the surrogate model, where local accuracy is desired. Even though the algorithm includes more points around the minimum, the biases of the large input space outweigh the increased fidelity near the optimal points. The standard deviation divided by average temperature is 0.029, below the threshold of 0.03 that was set in the optimization. This minor discrepency is again likely due to the limited accuracy of the surrogate model.

The energy use profile of the furrnace in these optimal results is such

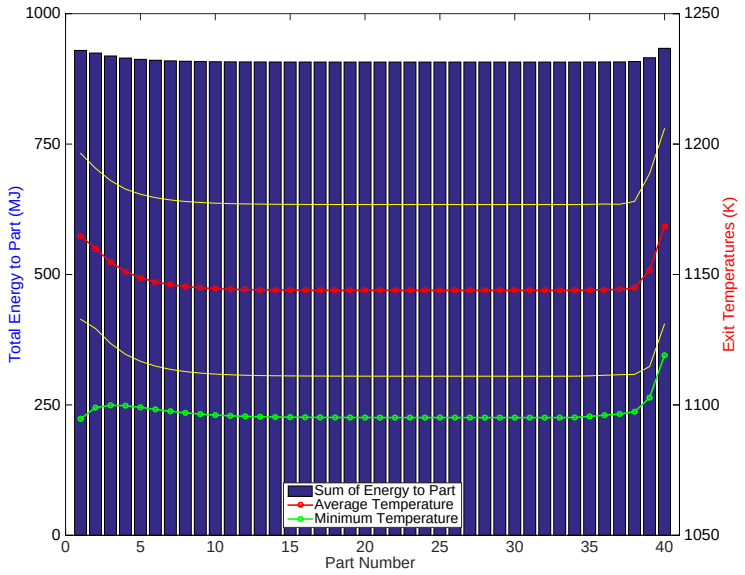

Figure 4.6: Part exit conditions for 40 parts in optimal operation. The yellow lines show the standard deviation around the average part temperature.

that the majority of the heating is done in zones 1 and 3. The heat to the part as a function of time, and thus position within the furnace, is show in Figure 4.7. We detail the heat to the part and temperature for part number 20. In this chart, the part is in each zone for one hour, so the hourly markings also correspond to the zone number. Even without a high set point in zone 1, the maximum amount of heating is done here as the driving force is the greatest. Zone 2 is still early enough in the heating process such that even with minimal heat input to the zone, some heating still occurs again due to the driving force. Additionally, since zones 1 and 3 are operating with high fuel flow rates, it is possible that radiative heat from the two zones bracketing zone 2 are heating the part, rather than the burners in zone 2 directly influencing

the heating. Zone 3 is responsible for the remainder of the heating to the part that needs to be performed. Zone 4 is where the temperature deviation shrinks. The deviation is primarily in the maximum temperature being much greater than average and minimum temperatures. Note the rise of the maximum temperature to $1500K$ after the third hour, and the large drop to $1200K$ in the course of 1 hour. The maximum temperature is on the part surface, which changes more rapidly than the average and minimum temperatures due to direct interactions with the burners.

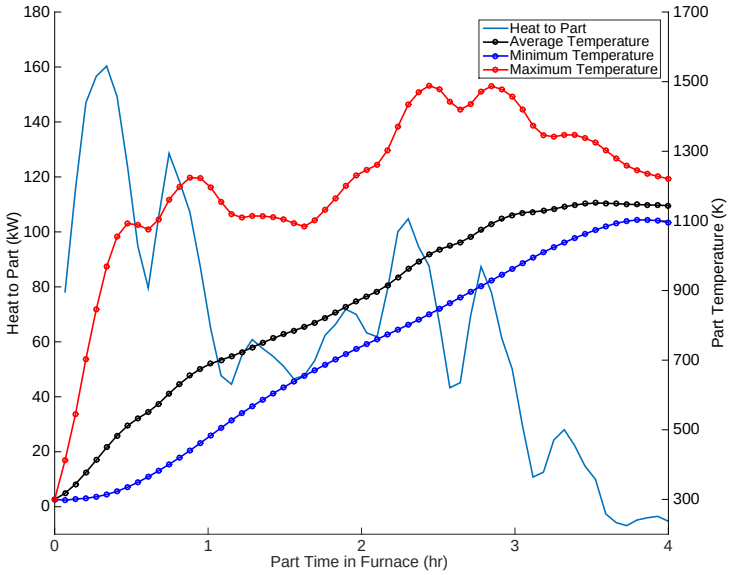

Figure 4.7: Heat input to the part and temperatures for part 20 with time in the furnace (and thus position) for optimal inputs. Most of the heating is accomplished in zones 1 and 3.

As shown by the response surface plots (Figure 4.4), a driving factor for zones 2 and 4 being set at the minimum allowed temperature set point is

to control the standard deviation. Recall from this figure that when zones 2 and 4 are set at $800K$, the resulting temperature standard deviation of the part will be minimal regardless of the set point of zones 1 and 3. As seen in Figure 4.7, the maximum temperature rises quickly in zones 1 and 3, and steadies in zone 2 while decreasing in zone 4. The rate of increase in the average temperature and minimum temperatures are not strongly influenced by the decrease in heat flux to the part. In these zones of the furnace, internal conduction within the part increases the average and minimum temperature. These zones allow for the maximum temperature (skin temperature) to settle, while the core temperatures continue to increase and approach the maximum temperature.

The optimized set point results are significantly different from the heuristic results in zone set points, but were designed to meet part exit standards without any excess. The primary difference is that zones 2 and 4 are set to the minimum temperature, instead of having a continuous increase in temperature set point throughout the furnace. More interesting is the energy use between heuristic and optimal set points, which we delve into with the next section.

4.3 Energy Efficiency Comparison

The overall goal of modeling and optimizing the system is to decrease the energy consumption within the furnace concerning the phenomena occuring within the system and of the condition of the parts is limited. Experience in running the plant has allowed the operators to know what 'works.' We have developed a framework of approximating the operation of the roller hearth furnace with a model, then using the model to find the optimal (i.e., least

energy intesive) method to operate the furnace.

Here, we compare three different scenarios in terms of energy consumption: the two temperature controlled operation scenarios shown in this chapter, and an optimized constant fuel operation in line with the results presented in Section 2.3. The optimal constant fuel input is found in the same manner as the optimization done in Section 4.2, but by using fuel flow rates as system inputs instead of zone temperature set points, in effect operating without closed-loop temperature control. In a sense, this would be controlling the fuel flow rate to the burners to a pre-specified set point.

Our key energy metric is total energy input to the system per part. We want to minimize this metric, while achieving desired part properties. A comparison of the energy usage in the three operation modes is shown in Table 4.2.

Heat Sources and Sinks	**Heuristic Set Points**	**Optimized Set Points**	**Optimized Fuel Flow**
Total Energy in Per Part	$29.5GJ$	$27.0GJ$	$26.4GJ$
Part Minimum Temperature	$1182K$	$1095K$	$1082K$
Part Standard Deviation	44.7	32.9	33.0
Energy to Parts (%)	27.2%	26.9%	26.9%
Energy Out the Exhaust (%)	50.0%	50.0%	50.0%
Energy to Flowing Nitrogen (%)	19.5%	19.8%	19.8%
Energy Thehrough Insulation (%)	3.3%	3.3%	3.3%

Table 4.2: Total energy input per part heated for three operation modes. We also show the energy distribution for these modes for the heat input for the operation modes. Note that the optimized results consider the same part exit qualities, while the heuristic set points do not.

In framing the objective in this manner, the heat-to-part efficiency metric is only implicitly valued; while an operating mode may have a greater

heat-to-part efficiency (how much heat from the burners is transferred to the part), we are more concerned with total energy use rather than the distribution of heat in the furnace. This is evident when comparing heuristic set points with optimized set points. The heuristic set points achieve greater energy to part efficiency, but this comes at the price of a greater amount of overall energy input. We note that in comparing these two modes, 8.5% less energy is input to the system by switching from the heuristic set points to optimized set points. Much of the energy savings can be seen by the difference in minimum temperature, where the heuristic mode gives minimum temperatures of $1182K$, while the optimized case is very close to the desired value of $1095K$.

There is an additional 2% energy savings when comparing optimized set points with optimized fuel flow rates. The optimized total fuel flow levels to each zone were found to be $[2.18, 0.40, 2.18, 0.40]\, kg/s$ where the fuel within each zone was distributed as 2/3 to the ceiling burners and 1/3 to the floor burners. These levels match the optimal furnace conditions for the temperature controlled case, where heating occurs in the first and third zone and minimal fuel is input to the second and fourth zones. Due to a lack of temperature control, with this method, it is possible for the temperatures within the furnace to breach certain limits. Constant fuel flow simulations have longer settling times, i.e. more parts needed to be processed before steady state input/output behavior is reached. The similar heat distributions between the optimized set points and optimized fuel flows suggests these two operating modes are largely equivalent in terms of how energy is inputted into the system. The additional energy savings can be reconciled with the fact that the parts did not achieve the proper exit temperature in this case either, where the minimum exit temperature for these fuel flow rates is $1082K$, $18K$ off the

target of $1100K$ while the optimized zone temperatures case was only $5K$ off target.

Chapter 5

Future Work and Conclusion

5.1 Future Work

Improvements to the response surface generation is one area to examine. We note local inaccuracies in our predicted outputs from the response surface, which we attribute to biases from the inclusion of the entire input space. To circumvent this, local sub-surrogate models of regions of interest (e.g. around the optimal point) would provide higher accuracy. Doing so, we believe there would not be an offset in the outputs found from the surrogate model to the actual results of the simulation.

We look to expand this work past real-time optimization to further techniques for energy savings, such as model predictive control (MPC). While the real-time optimization work shown here has shown potential for passive energy savings, we see MPC as a technique to further decrease energy use from active monitoring of the system. We aim to vary the temperature set points of the furnace during operation to achieve increased energy savings. Since the system operates with a known disturbance from parts entering and exiting the furnace, we expect that feedforward control would handle these instances optimally from an energy standpoint.

Validation of the model will occur once plant data becomes available. We anticipate the plant process data to include operating conditions such as furnace temperatures, fuel flow rates, and the mass throughput of steel. We

are confident that our model can be adjusted to match the furnace operating conditions by varying insulating wall parameters such as thickness, thermal conductivity, and emissivity.

Concerning the steel parts, the plant samples a small number of parts in each batch after the austenitization furnace and oil quench process is complete to test for part quality of the entire batch. While part exit temperature will not be explicitly measured from this sampling, we expect other metrics obtained (hardness, shear strength, and tensile strength, for example) of the sampled steel to be useful in approximating exit conditions, which can then suggest updated operating parameters for the next run. Correlating sample quality to overall batch conditions for run-to-run control purposes mirrors developments in semiconductor manufacturing where virutal metrology is used. Virtual metrology (see Edgar et al. [2000] for a survey) is a method of process monitoring where select parts from a batch are measured to approximate desired properties (e.g. thickness) of the entire batch. Using inferred knowledge of the previous run, statistical methods can then be used to guide control decisions for the next run. We see potential for applying tests from virtual metrology for semiconductor manufacturing are applicable to the roller hearth furnace operation.

An additional means to assist in obtaining steel process conditions would involve heating a "datapack" (a heat resistant temperature probe) in the furnace with the steel parts. The datapack would record temperatures while within in the furnace. While this would only be done in experimental settings rather than with each run, the datapack would be informative for knowledge of how the temperature profile of the part varies with time and position in the furnace. From these studies, we anticipate tuning steel part

parameters in the model such as thermal diffusivity and emissivity to match the conditions found in experiments. We also look to vary the shape of the part in the simulation to explore different surface area to volume ratios. Doing so will approximate the plant more accurately, where a tray of up to 40 steel parts are heated, rather than a rectangular slab.

5.2 Conclusion

In this thesis, a two-dimensional energy focused model of a roller hearth furnace was developed. Radiation heat transfer was described using a radiosity-based approach due to strong surface-to-surface interactions. The model can compute the exit temperature profile of a steel part that passes through the furnace while calculating the energy consumption and efficiency of the furnace. We proposed a dual iterative scheme, alternating between estimating heat fluxes to the discretized furnace surfaces, and estimating the temperature within the parts, to solve the furnace model.

Temperature feedback control of the furnace was then implemented, where the temperature is controlled by manipulating the fuel flow rate to the burners. We used this framework first to examine energy consumption within the furnace for operator-specified heuristic temperature set points, then to find the optimal set points to minimize energy consumption while ensuring specified part exit conditions. We first developed surrogate models to approximate the complex physics-based model with algebraic equations relating the outputs to the inputs. The optimization scheme then used the surrogate models of the outputs to find the set points that heat the parts to the desired temperature conditions while minimizing energy consumption. The use of modeling and optimization of the system resulted in theoretical energy savings of 8.5% when

comparing our optimized case with the heuristic case.

We see the work done in this real-time optimization study as an additional tool in operation of the furnace. The detailed model and finding of optimal set points will provide additional insights for the operators. With added information of the process, the plant will be able to make proper decisions in the overall goal of decreasing energy utilization.

Appendix

Appendix 1

Notation

Variable	Description
A_i	Area for surface i $[m^2]$
AFR	Air-Fuel Ratio within burner
β_j	Least squares regression coefficient
$C_{p,blended}$	Average heat capacity for exhaust gases $[J/(kg * K)]$
ϵ_i	Emissivity for surface i
$F_{i,j}$	View factor from surface i to j
h_{loc}	Heat transfer coefficient for specified location $[W/(m^2 * K)]$
h^{ent}	Temperature dependent specific enthalpy $[KJ/mol]$
ΔH_{comb}	Heat of combustion $[KJ/mol]$
$H(T_w^\infty)$	Enthalpy based on temperature T_w^∞ $[KJ/mol]$
$G(\frac{Q_{w+1}}{\dot{m}})$	Temperature based on enthalpy and mass flow rate of fluid in control volume $w+1$ $[K]$
i	Index for furnace subsurface
J_i	Radiosity for surface i $[W/m^2]$
K	Index for control volume within furnace
$\dot{m}_{N_2}$	Mass flow rate of blanket nitrogen $[kg/s]$
$\dot{m}_{fuel}$	Mass flow rate of combustion gas through burner $[kg/s]$
N	Total number of surface for furnace
Q_w	Current heat of zone w $[W]$
$Q_{net,i}$	Total heat from surface i $[W]$
$Q_{radiation,i}$	Total radiation from surface i $[W]$
$Q_{convection,i}$	Total convection from surface i $[W]$
T_i	Temperature for surface i $[K]$
T_{in}	Inlet temperature to burner $[K]$
T_w^∞	Temperature air in zone w $[K]$
$X_j(u)$	Surrogate model basis function

Bibliography

H Akaike. Factor analysis and aic. Psychometrika, 52(3):317–332, 1987.

TA Badgwell, T Breedijk, SG Bushman, SW Butler, S Chatterjee, TF Edgar, AJ Toprac, and I Trachtenberg. Modeling and control of microelectronics materials processing. Computers & chemical engineering, 19(1):1–41, 1995.

L Balbis, J Balderud, and MJ Grimble. Nonlinear predictive control of steel slab reheating furnace. In American Control Conference, 2008, pages 1679–1684. IEEE, 2008.

WH Chen, YC Chung, and JL Liu. Analysis on energy consumption and performance of reheating furnaces in a hot strip mill. International Communications in Heat and Mass Transfer, 32(5):695–706, 2005.

Alison Cozad, Nikolaos V Sahinidis, and David C Miller. Learning surrogate models for simulation-based optimization. AIChE Journal, 60(6):2211–2227, 2014.

GH Derrick. A three-dimensional analogue of the hottel string construction for radiation transfer. Journal of Modern Optics, 32(1):39–60, 1985.

Thomas F Edgar, Stephanie W Butler, W Jarrett Campbell, Carlos Pfeiffer, Christopher Bode, Sung Bo Hwang, KS Balakrishnan, and Juergen Hahn. Automatic control in microelectronics manufacturing: Practices, challenges, and possibilities. Automatica, 36(11):1567–1603, 2000.

SH Han, D Chang, and C Huh. Efficiency analysis of radiative slab heating in a walking-beam-type reheating furnace. Energy, 36(2):1265–1272, 2011.

CA Henao and CT Maravelias. Surrogate-based superstructure optimization framework. AIChE Journal, 57(5):1216–1232, 2011.

AFC Holcroft. Conveyor Furnaces: Continuous Conveyor Thermal Treatment System. `http://www.afc-holcroft.com/userfiles/file/pdf/ConveyorFurnace_Brochure.pdf`. Accessed: 2015-04-09.

JR Howell. The monte carlo method in radiative heat transfer. Journal of Heat Transfer, 120(3):547–560, 1998.

FP Incropera. Fundamentals of heat and mass transfer. John Wiley & Sons, 2011.

A Jaklič, F Vode, and T Kolenko. Online simulation model of the slab-reheating process in a pusher-type furnace. Applied Thermal Engineering, 27(5):1105–1114, 2007.

D Kang, Y Kim, Y Kim, W Kim, and K Kim. Experimental and numerical studies on the thermal analysis of the plate in indirectly-fired continuous heat treatment furnace. VDI BERICHTE, 1988:533, 2007.

J Kang and Y Rong. Modeling and simulation of load heating in heat treatment furnaces. Journal of materials processing technology, 174(1):109–114, 2006.

JG Kim, KY Huh, and IT Kim. Three-dimensional analysis of the walking-beam-type slab reheating furnace in hot strip mills. Numerical Heat Transfer: Part A: Applications, 38(6):589–609, 2000.

YI Kim, KC Moon, BS Kang, C Han, and KS Chang. Application of neural network to the supervisory control of a reheating furnace in the steel industry. Control Engineering Practice, 6(8):1009–1014, 1998.

P Laurinen and J Röning. An adaptive neural network model for predicting the post roughing mill temperature of steel slabs in the reheating furnace. Journal of materials processing technology, 168(3):423–430, 2005.

Y Liao, M Wu, and JH She. Modeling of reheating-furnace dynamics using neural network based on improved sequential-learning algorithm. In Computer Aided Control System Design, 2006 IEEE International Conference on Control Applications, 2006 IEEE International Symposium on Intelligent Control, 2006 IEEE, pages 3175–3181. IEEE, 2006.

A Mochida, K Kudo, Y Mizutani, M Hattori, and Y Nakamura. Transient heat transfer analysis in vacuum furnaces heated by radiant tube burners. Energy conversion and management, 38(10):1169–1176, 1997.

RH Myers, DC Montgomery, and CM Anderson-Cook. Response surface methodology: process and product optimization using designed experiments, volume 705. John Wiley & Sons, 2009.

M Niederer, S Strommer, A Steinboeck, and A Kugi. A simple control-oriented model of an indirect-fired strip annealing furnace. International Journal of Heat and Mass Transfer, 78:557–570, 2014.

J Pan, Y Li, and D Li. The application of computer simulation in the heat-treatment process of a large-scale bearing roller. Journal of materials processing technology, 122(2):241–248, 2002.

V Panjkovic and R Gloss. Fast dynamic heat and mass balance model of walking beam reheat furnace with two-dimensional slab temperature profile. Ironmaking & Steelmaking, 39(3):190–209, 2012.

JL Pellegrino, N Margolis, M Justiniano, M Miller, and A Thekdi. Energy use, loss and opportunities analysis. Technical report, Energetics, Incorporated and E3M, Incorporated, 2004.

HE Pike Jr and SJ Citron. Optimization studies of a slab reheating furnace. Automatica, 6(1):41–50, 1970.

H Ramamurthy, S Ramadhyani, and R Viskanta. A thermal system model for a radiant-tube continuous reheating furnace. Journal of materials engineering and performance, 4(5):519–531, 1995.

D Seborg, TF Edgar, and D Mellichamp. Process dynamics & control. John Wiley & Sons, 2004.

A Steinboeck, D Wild, T Kiefer, and A Kugi. A mathematical model of a slab reheating furnace with radiative heat transfer and non-participating gaseous media. International Journal of Heat and Mass Transfer, 53(25):5933–5946, 2010.

A Steinboeck, K Graichen, and A Kugi. Dynamic optimization of a slab reheating furnace with consistent approximation of control variables. Control Systems Technology, IEEE Transactions on, 19(6):1444–1456, 2011.

A Steinboeck, D Wild, and A Kugi. Nonlinear model predictive control of a continuous slab reheating furnace. Control Engineering Practice, 21(4): 495–508, 2013.

EJ Stones, KA Ferland, and M Noack. Industrial efficiency. Technical report, NPC Global Oil and Gas Study, 2007.

Y Tang, J Laine, T Fabritus, and J Harkki. Different methods obtained by PHOENICS simulation to improve the performance of pusher-type steel slab reheating furnace. Oulu University, 2010.

A Thekdi. Energy efficiency improvement opportunities in process heating for the forging industry. E3M, 2010.

R Tibshirani. Regression shrinkage and selection via the lasso. Journal of the Royal Statistical Society. Series B (Methodological), pages 267–288, 1996.

MK Tiwari, A Mukhopadhyay, and D Sanyal. Process modeling for control of a batch heat treatment furnace with low no¡ sub¿ x¡/sub¿ radiant tube burner. Energy conversion and management, 46(13):2093–2113, 2005.

DC Triebl, C Spijker, H Raupenstrauch, A Jarosik, and G Angeli. Cfd-simulation eines direkt befeuerten ofens zur vorbehandlung feuerverzinkter stahlbänder. BHM Berg-und Hüttenmännische Monatshefte, 159(7):310–311, 2014.

United States Energy Information Administration. Monthly energy review November 2014. Accessed Dec 15, 2014, 2014.

V Viswanathan, R Davies, and J Holbery. Opportunity analysis for recovering energy from industrial waste heat and emissions. Pacific Northwest National Laboratory, 2005.

A Wächter and LT Biegler. On the implementation of an interior-point filter line-search algorithm for large-scale nonlinear programming. Mathematical programming, 106(1):25–57, 2006.

S Xuegang, Y Chao, and C Yihui. Dynamic modeling of reheat-furnace using neural network based on pso algorithm. In Mechatronics and Automation, 2009. ICMA 2009. International Conference on, pages 3097–3101. IEEE, 2009.

Y Yang and Y Lu. Development of a computer control model for slab reheating furnaces. Computers in Industry, 7(2):145–154, 1986.

Y Yang and Y Lu. Dynamic model based optimization control for reheating furnaces. Computers in industry, 10(1):11–20, 1988.

N Yoshitani, T Ueyama, and M Usui. Optimal slab heating control with temperature trajectory optimization. In Industrial Electronics, Control and Instrumentation, 1994. IECON'94., 20th International Conference on, volume 3, pages 1567–1572. IEEE, 1994.

B Zhang, Z Chen, L Xu, J Wang, J Zhang, and H Shao. The modeling and control of a reheating furnace. In American Control Conference, 2002. Proceedings of the 2002, volume 5, pages 3823–3828. IEEE, 2002.

Vita

Vincent Roathy Heng was born in San Diego, California on 19 July 1991. He graduated Mt Carmel High School in San Diego in 2009. Immediately after high school, Vincent attended the University of California, Los Angeles, where he achieved a Bachelor of Science in Chemical Engineering in June, 2013. Vincent continued his academic streak when he enrolled in the University of Texas at Austin in the McKetta Department of Chemical Engineering of the Cockrell School of Engineering for graduate school in September of 2013.

Permanent address: 8904 Polanco St
San Diego, California 92129

This thesis was typeset with LaTeX[†] by the author.

[†]LaTeX is a document preparation system developed by Leslie Lamport as a special version of Donald Knuth's TeX Program.